Eur. Phys. J. D **38**, 545–552 (2006)
DOI: 10.1140/epjd/e2006-00065-7

THE EUROPEAN PHYSICAL JOURNAL D

A rubidium-stabilized ring-cavity resonator for optical frequency metrology: precise measurement of the D_1 line in ^{133}Cs

D. Das, A. Banerjee, S. Barthwal, and V. Natarajan[a]

Department of Physics, Indian Institute of Science, 560012 Bangalore, India

Received 19 October 2005 / Received in final form 30 December 2005
Published online 28 March 2006 –

Abstract. We have developed a ring-cavity resonator that can be used to measure the absolute frequencies of optical transitions with an uncertainty below 40 kHz. The length of the resonator is calibrated against a reference laser locked to the D_2 line of ^{87}Rb, the frequency of which is known with 6 kHz accuracy. We demonstrate the power of this technique by measuring the absolute frequencies of various hyperfine transitions in the D_1 line of ^{133}Cs. Our results agree with earlier measurements using the frequency-comb technique, and have similar accuracy. Measurement of the D_1-line frequency could lead to a more precise determination of the fine-structure constant. We also report a precise value of $A = 291.918(8)$ MHz for the hyperfine constant in the $6P_{1/2}$ state.

PACS. 06.30.Ft Time and frequency – 42.62.Eh Metrological applications; optical frequency synthesizers for precision spectroscopy – 32.10.Fn Fine and hyperfine structure

1 Introduction

High-precision measurements of atomic energy levels have played an important role in the development of physics. The most notable example is the measurement of the Lamb shift of the 2P state of hydrogen, which led to the birth of quantum electrodynamics. In recent years, the energy levels of alkali atoms have become particularly important because these atoms can be laser cooled to ultra-low temperatures [1] for further use in high-resolution spectroscopy experiments. For example, precise measurements of the D_1 lines in Cs [2], Rb, and K [3], combined with measurements of the photon-recoil shift using laser-cooled atoms in an atom interferometer [4] and precise mass measurements in a Penning trap [5], could lead to a new high-precision determination of the fine-structure constant α. Furthermore, a precise value of the frequency of the D_2 line in Cs [6,7] is required for atom-interferometric measurements of the local gravitational acceleration [8]. Heavy alkali atoms are also being used in sensitive measurements of discrete-symmetry violations in the laws of physics, such as parity [9] and time-reversal symmetry [10]. In these experiments, it becomes necessary to make a careful comparison of the experimental data with theoretical predictions. Precise measurements of hyperfine-structure and isotope-shifts in atomic lines can help in fine-tuning the atomic wavefunction used in such calculations, especially in accounting for the contribution from nuclear interactions.

In this article, we describe in detail a technique for measuring the absolute frequency of optical transitions with <40 kHz accuracy. Recently, the smallest errors in frequency measurements have been reported using the frequency-comb technique. For example, uncertainty of <50 kHz has been achieved for measurements on the D lines of Cs using this technique [2,7]. In these cases, the width of the resonance line itself limits the obtained accuracy. Our relatively simpler technique offers similar accuracy in such measurements. In addition, we can verify our estimate of systematic errors by varying the reference frequency over a narrow range. Other techniques for frequency measurement, such as the use of Fabry-Perot cavities [11], acousto-optic modulators [12], level-crossing [13] and optical double-resonance spectroscopy [14], have accuracy limited to about 1 MHz.

The technique described here combines the advantages of using tunable diode lasers to access atomic transitions with the fact that the absolute frequency of the D_2 line in ^{87}Rb has been measured with an accuracy of 6 kHz [15]. A frequency-stabilized diode laser locked to this line is used as a frequency reference, along with a ring-cavity resonator whose length is locked to the reference laser. For a given cavity length, an unknown laser locked to an atomic transition has a small frequency offset from the nearest cavity resonance. This offset is combined with the cavity mode number to obtain a precise value for the frequency of the unknown laser. We have earlier used this technique to make precise measurements of the absolute frequencies of the D_1 lines in ^{39}K, ^{85}Rb, and ^{87}Rb [3], D_2 lines in ^{85}Rb [16] and ^{39}K [17], and isotope shifts and hyperfine

[a] e-mail: vasant@physics.iisc.ernet.in

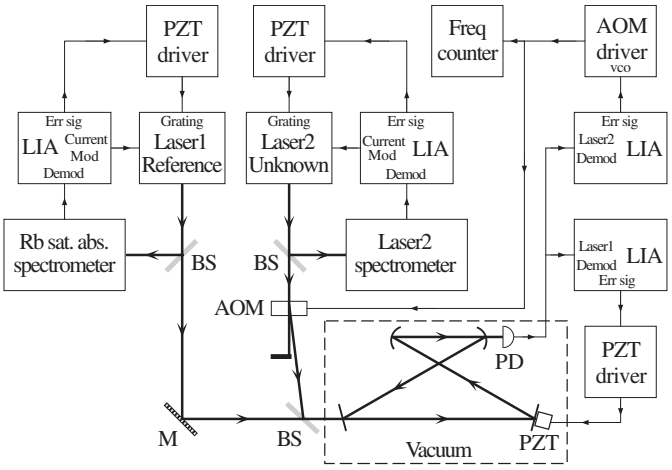

Fig. 1. Schematic of the experiment. Figure key – LIA: lock-in amplifier, PZT: piezoelectric transducer, AOM: acousto-optic modulator, BS: beam splitter, M: mirror, PD: photodiode.

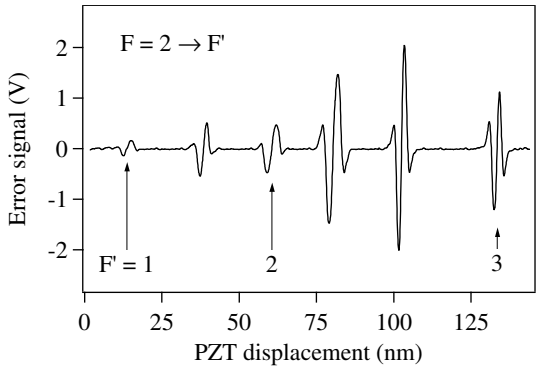

Fig. 2. Error signal. The trace is the third-derivative error signal as a function of displacement of the feedback grating in the reference laser (D_2 line of ^{87}Rb). The hyperfine peaks are labelled with the value of F', while the peaks in between are crossover resonances.

structure of the 398.8 nm line in Yb [18,19]. In this paper, we apply the technique to measure the frequencies of various hyperfine transitions in the D_1 line in ^{133}Cs. Our results agree very well with previous measurements using the frequency-comb technique [2].

As mentioned before, frequency measurements have been done previously using a linear Fabry-Perot resonator, with a stabilized HeNe laser as the frequency reference [11]. Our use of a Rb-stabilized diode laser as the reference has the primary advantage that there are several known hyperfine transitions that can be used for locking the laser. This enables us to check for certain kinds of systematic errors that arise in difference-frequency measurements. Another advantage of the ring-cavity design is that diffraction effects are wavelength independent, as we will see later. Furthermore, the ring cavity has a travelling wave inside and there is no possibility of feedback destabilization of the laser. The design is very compact and the cavity is easily temperature controlled to increase its passive stability.

2 Experimental details

The schematic of the experiment is shown in Figure 1. The experiment uses two frequency-stabilized diode lasers that are locked to atomic transitions using Doppler-free saturated-absorption spectroscopy. Laser1 is the reference laser locked to the D_2 line of ^{87}Rb. Laser2 is the unknown laser, which in this case is locked to the D_1 line of ^{133}Cs. The output of the two lasers is coupled into the ring-cavity resonator. The cavity length is adjusted using a piezo-mounted mirror to bring it into resonance with the wavelength of Laser1. The cavity is then locked to this length in a feedback loop. However, Laser2 will generally be offset from the cavity resonance. This offset is accounted for by shifting the frequency of the laser using an acousto-optic modulator (AOM) before it enters the cavity. The error signal between the shifted frequency of Laser2 and the cavity resonance is fed back to the AOM driver which locks the AOM frequency at the correct offset. The AOM frequency is read using a frequency counter. The absolute frequency of Laser1 is known with 6 kHz accuracy [15], therefore, once the cavity length (or mode number) is known, the frequency of Laser2 is determined very precisely.

The diode laser system used as the reference laser (Laser1) is built around a commercial single-mode laser diode with a nominal operating wavelength of 785 nm and output power of 25 mW. The laser is frequency stabilized in a standard external-cavity design using optical feedback from an 1800 lines/mm diffraction grating (Littrow configuration). The grating is mounted on a piezoelectric transducer for electronic tuning of the wavelength [20]. The short-term linewidth of the laser after stabilization has been measured to be below 500 kHz. A part of the output beam is tapped for saturated-absorption spectroscopy in a room-temperature Rb vapor cell (density $\sim 10^9$ atoms/cm^3). Using a combination of temperature and current control, the diode is tuned to the 780-nm D_2 line in ^{87}Rb ($5S_{1/2} \leftrightarrow 5P_{3/2}$ transition). It is then locked to one of the hyperfine peaks in the spectrum by modulating the injection current and using third-harmonic demodulation. Such third-harmonic detection produces narrow error signals that are free from effects due to the Doppler background or intensity fluctuations [21]. We have shown earlier that this locking technique fixes the laser frequency to within a few kHz of the peak center [16]. In Figure 2, we show a typical error signal as the laser is scanned across the $F = 2 \rightarrow F'$ transitions. All the peaks and crossover resonances are clearly resolved. The error signal is very symmetric about each peak center. Note that, over this large scan range, the laser frequency has a nonlinear dependence on piezo displacement.

Laser2 is a similar diode laser system operating at 895 nm for measurements on the D_1 line in Cs ($6S_{1/2} \leftrightarrow 6P_{1/2}$ transition). As in the case of the reference laser, this laser is locked to a particular hyperfine transition using saturated-absorption spectroscopy in a room-temperature Cs vapor cell (density 5×10^8 atoms/cm^3).

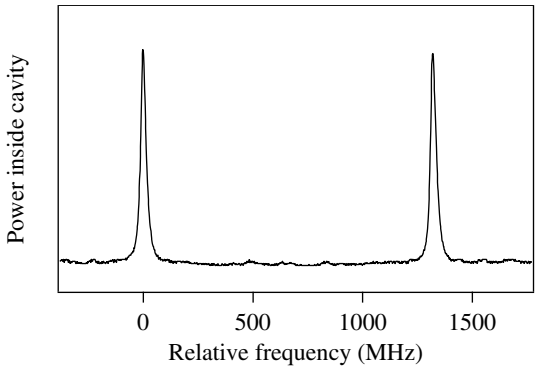

Fig. 3. Cavity modes. The figure shows the power coupled into the cavity as the frequency of the reference laser is scanned. The free-spectral range is 1322.63 MHz, and the width of each peak is 28 MHz.

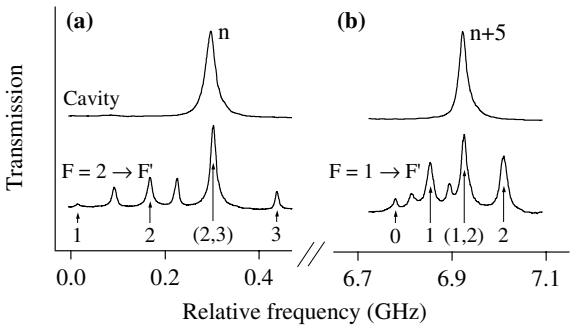

Fig. 4. The cavity fsr is determined by locking the cavity to the unknown laser and using two lock points for the reference laser: $F = 2 \rightarrow F' = (2, 3)$ shown in (a), and $F = 1 \rightarrow F' = (1, 2)$ shown in (b). The cavity mode number in (b) increases by exactly 5.

The ring cavity used for the frequency measurement consists of two plane mirrors and two concave mirrors in a bow-tie arrangement. The curved mirrors have radius of curvature of 25 mm. The mirrors have a dielectric coating that has a flat response over the range 760−900 nm. One of the plane mirrors is mounted on a piezoelectric transducer and is used to adjust the cavity length electronically. The piezoelectric transducer has a full deflection of 6.1 μm for a voltage of 150 V. The mirrors are mounted on ultra-stable kinematic mounts. The mounts are fixed to a copper plate that is temperature stabilized using a thermoelectric cooler to increase the passive stability of the cavity.

In order to determine the stable operating region of the cavity, we analyze the cavity using the standard **ABCD** matrices for Gaussian-beam propagation [22]. It is necessary to analyze the sagittal and tangential planes separately because of the 15° angle of incidence on the curved mirrors. The cavity modes are therefore elliptical. The cavity has two beam waists, a larger one between the plane mirrors and a smaller one between the curved mirrors [17]. For a cavity length of 226.5 mm and a path length of 26.5 mm between the curved mirrors, the larger beam waist has a $1/e^2$ diameter of 224×119 μm, while the smaller waist has a diameter of 13.8×13.4 μm (at 780 nm). The larger waist has a correspondingly larger Rayleigh range and is used for easy mode matching of the laser beams into the cavity. The output of the lasers is coupled into the cavity through a lens of $f = 50$ cm. This results in a coupling efficiency of about 15%, which is sufficient for ensuring stable locking to the cavity mode.

The measured cavity modes are shown in Figure 3, which is a plot of the power inside the cavity as a function of the laser frequency. Note that higher order modes of the cavity are extremely well suppressed. The free spectral range is 1.3 GHz, corresponding to a cavity length of 226.5 mm. The cavity modes have a width of about 28 MHz. The cavity is locked to the reference laser by feeding back the error signal to the piezo-mounted mirror. Since the modes appear on a flat background, the error signal is just the first-derivative signal. The width of the cavity modes is similar to the linewidth of atomic transitions used in laser stabilization, and one expects similar definition of the lock point. The relatively large width also ensures robust locking that is insensitive to perturbations over a wide dynamic range. Indeed, we have recently shown that such a ring-cavity resonator can be used to lock and scan a tunable laser for spectroscopy applications [23].

The most important aspect of the measurement is to fix the mode number of the cavity uniquely. This is done in two steps: we first measure the cavity free-spectral range (fsr) and then use a coarse measurement of the frequency of Laser2. The fsr measurement proceeds as follows. We lock the cavity with the reference laser on the $F = 2 \rightarrow F' = (2, 3)$ transition, as shown in Figure 4a, and measure the AOM offset for a given transition of the unknown laser. We then shift the reference laser to the $F = 1 \rightarrow F' = (1, 2)$ transition, which is exactly 6622.887 MHz higher [15, 24]. This shift causes the cavity mode number to increase by almost exactly 5, as shown in Figure 4b. The cavity is locked to the new frequency and the AOM offset for the same transition of the unknown laser is measured. The difference in the two AOM offsets along with the change in the reference frequency gives exactly 5 times the cavity fsr. Using this method, the fsr is determined with a precision of 20 kHz. The next step in determining the mode number is to get a coarse measurement of Laser2. For this, we use a home-built wavemeter [20] that gives the frequency with an uncertainty of 10 MHz. Thus, there is a unique mode number that matches the resonance condition for the two laser frequencies and the measured fsr. For example, at some cavity length L, this length matches the resonance condition $L = n\,\lambda$ with a mode number of $n_{\rm ref} = 289418$ for the reference laser locked to the $F = 2 \rightarrow F' = (2, 3)$ transition (frequency of 384 227 981.877 MHz). The same length also matches the resonance condition for the unknown laser with a mode number of $n_{\rm unk} = 252422$ when the laser frequency is AOM-downshifted by exactly 16.784 MHz from the $F = 4 \rightarrow F' = 4$ transition of the Cs D_1 line. Thus the unknown frequency of this transition is determined to be 335 112 537.917 MHz. The fsr at this length is 1327.588 MHz. The next nearest mode satisfying the

resonance condition has an fsr differing by 350 kHz, or 17 times the error in the determination of the fsr.

3 Error analysis

3.1 Statistical errors

The primary sources of statistical error in our technique are fluctuations in the lock points of the lasers, the cavity, and the AOM. To minimize such effects, we use an integration time of 10 s in the frequency counter during each measurement of the AOM offset. We then take an average of about 50 measurements for a given transition. This results in an overall statistical error of less than 5 kHz in each value. The timebase in the frequency counter used to measure the AOM frequency has a stability of better than 10^{-6}, which translates to a negligible error of 100 Hz in the frequency measurement.

3.2 Systematic errors

There are two classes of potential systematic errors that we have considered. The first class of errors comes from systematic shifts in the laser frequencies. The second class of errors is inherent to our technique because we are really comparing the wavelength (and not the frequency) of the two lasers, and hence we have to account for possible dispersion effects. Let us first consider the shift in the lock points of the lasers.

3.2.1 Shift of the reference laser

(i) Shift in the peak position can occur due to (a) optical-pumping effects and (b) velocity redistribution of the atoms in the vapor cell due to radiation pressure [25]. Such effects manifest themselves as inversion of hyperfine peaks or distortion of the Lorentzian lineshape. We minimize these effects by using very low intensities of the pump and probe beams in the saturated-absorption spectrometer. The typical intensity in the probe beam is about 0.25 mW/cm^2 compared to the saturation intensity of 1.64 mW/cm^2. The pump beam has an intensity 3 times higher. The shape of the error signals in Figure 2 shows that our peaks have symmetric lineshapes.

(ii) Line shifts from stray magnetic fields in the vicinity of the cells. The primary effect of a magnetic field is to split the Zeeman sublevels and broaden the line without affecting the line center. However, line shifts can occur if there is asymmetric optical pumping into Zeeman sublevels. For a transition $(F, m_F) \rightarrow (F', m_{F'})$, the systematic shift of the line center is $\mu_B(g_{F'}m_{F'} - g_F m_F)B$, where $\mu_B = 1.4$ MHz/G is the Bohr magneton, g's denote the Landé g factors of the two levels, and B is the magnetic field. The selection rule for dipole transitions is $\Delta m = 0, \pm 1$, depending on the direction of the magnetic field (quantization axis) and the polarization of the light. Thus, if the beams are perfectly linearly polarized, there will be no asymmetric driving and the line center is not affected. We therefore use linearly polarized light to reduce these effects. We further verify that the effects are negligible by repeating the measurements at different locations in the laboratory, and with and without the use of a magnetic shield around the cell.

(iii) Shift in the lock point due to the underlying Doppler profile, peak-pulling from nearby transitions, or phase shifts in the feedback loop. We minimize the first two effects by using third-harmonic detection for the error signal.

(iv) Collisional shifts in the vapor cell. The pressure inside the cell is 0.2 mtorr, and we estimate the shift to be less than 10 kHz. To further verify this, we repeat the measurements with cells from different manufacturers (which have different background contamination) and find no significant difference.

3.2.2 Shift of the Cs laser

For the Cs D_1 line, the effects of radiation pressure and collisional shifts considered above are similarly negligible. The typical intensity in the probe beam is 0.20 mW/cm^2, which is again much smaller than the saturation intensity of 0.83 mW/cm^2. The most important effects come from optical pumping and stray magnetic fields. For the saturated-absorption spectroscopy, we have chosen the lin $\perp$ lin configuration, i.e. a configuration with orthogonal linear polarizations for the pump and probe beams. This configuration allows us to use polarizing-beamsplitter cubes so that the counterpropagating beams have only a small misalignment angle between them. In addition, the extinction ratio of better than 1000:1 in the cubes ensures near-perfect linear polarization of the beams, which makes it less susceptible to optical-pumping effects. We further reduce stray-field effects by using a magnetic shield [26] around the cell to reduce the field below 5 mG. The shifts due to this magnetic field are different for different transitions, and vary in size from 2 to 9 kHz.

The observed spectrum for one of the peaks in the D_1 line is shown in Figure 5. The relatively large hyperfine interval in the excited state means that the Doppler profiles of the individual transitions are non-overlapping and there are no crossover resonances. Each saturated-absorption peak appears exactly at the bottom of its Doppler-broadened line. In order to ensure that the frequency-scan axis in Figure 5 is perfectly linear, the spectrum is obtained by double passing the laser beam through an AOM and scanning the AOM frequency. The scan width is limited by the AOM bandwidth. The solid line is a Lorentzian fit, which fits the spectrum extremely well and shows that the lineshape is symmetric. The fit yields a linewidth of 11 MHz, which is somewhat larger than the natural linewidth of 5 MHz. This increase is typical in saturated-absorption spectroscopy, and is primarily caused by a small misalignment angle between the

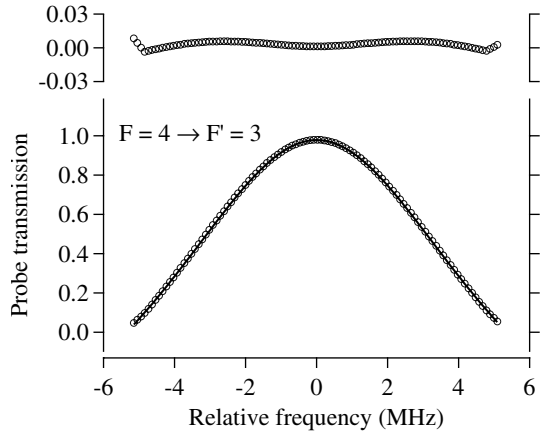

Fig. 5. Saturated-absorption spectrum in the D_1 line. The open circles represent the measured probe-transmission signal (normalized) around the $F = 4 \rightarrow F' = 3$ peak. The solid line is a Lorentzian fit, with the residuals shown on top.

counter-propagating beams and power broadening from the pump beam.

3.2.3 Dispersion effects

One important source of systematic errors arises due to dispersion of the medium inside the cavity, which is eliminated by using an evacuated cavity. At a pressure of 10^{-2} torr, the refractive indices are the same to better than one part in 10^{11}. However, there could be wavelength-dependent phase shifts at the dielectric-coated mirrors used in the cavity. If there is an additional phase shift of ϕ in one round trip in the cavity, the resonance condition for a cavity of length L becomes

$$2n\pi = kL + \phi, \tag{1}$$

where n is an integer and k is the wavevector. This could lead to a systematic error if ϕ is different for the reference and unknown wavelengths. We check for such errors by repeating the measurement at two cavity lengths, L_1 and L_2. If there is a differential phase shift at the mirrors between the two wavelengths, then it can be shown that

$$f_0 = \frac{f_1 L_1 - f_2 L_2}{L_1 - L_2}, \tag{2}$$

where f_1 (f_2) is the frequency measured at L_1 (L_2), and f_0 is the correct frequency. Basically, the error due to the differential phase shift is the same at the two cavity lengths, while the accumulated phase due to the wave propagation increases with the length. To minimize this error, we use mirrors that have a flat reflectivity over a large wavelength range. This is in contrast to high-finesse cavities used in measurements with HeNe lasers where the mirror reflectivity falls off quite sharply away from the HeNe center frequency. The dispersion effects in such cavities are generally much higher.

It is also important to note that this class of wavelength-dependent systematic errors does not affect the determination of *frequency differences* of the unknown laser, up to several 10s of GHz. This is the order of magnitude of frequency differences that arise when determining hyperfine structure or isotope shifts. Thus, our technique is well suited for such measurements.

3.2.4 Diffraction effects

Diffraction effects inside the cavity appear as an additional (Guoy) phase as the beam propagates through a cavity waist. These effects can be quite important in interferometers and wavemeters. The Guoy phase is given by [27] $\arctan(z/z_R)$, where z is the propagation distance and $z_R = \pi w_0^2/\lambda$ is the Rayleigh range around a waist of radius w_0. In our cavity, the **ABCD** matrix analysis shows that the two waist sizes are proportional to $\sqrt{\lambda/\pi}$ [17]. Therefore, the Rayleigh ranges are identical for all wavelengths, and so is the Guoy phase. In effect, the concave mirrors in the cavity impose a boundary condition on the wavefront curvature at their locations, and this ensures that the Rayleigh ranges are independent of wavelength. Thus one does not expect any systematic error due to this effect. This is an important advantage of the ring-cavity design.

3.2.5 Other effects

An important source of error in wavemeters based on a scanning Michelson interferometer, as described in our earlier work [20], is the geometric alignment of the reference and unknown beams into the interferometer. Any misalignment angle between the beams would change the measured wavelength. By contrast, the cavity technique used in the current work is completely insensitive to geometric factors. The geometric alignment of the beam determines (very sensitively) the degree of mode matching into the cavity, but the cavity resonance condition depends only on the wavelength. Furthermore, we check the mode structure to verify that higher-order cavity modes are not excited significantly (see Fig. 3), which could cause peak pulling of the fundamental mode.

3.2.6 Summary

The estimated size of the different sources of systematic error for the reference laser on the Rb D_2 line and the unknown laser on the Cs D_1 line are listed in Table 1.

The numbers listed in Table 1 are our estimates for these errors. However, we have several experimental handles to verify that these errors are reasonable. In particular, the total error can be measured directly. As mentioned in the introduction, this ability to verify systematic errors is one of the primary advantages of our technique. For the reference laser, we check the total error by measuring the same unknown frequency using different hyperfine peaks to lock the reference laser. The reference frequency changes by up to several GHz, but these changes are

Table 1. Error budget.

Source of error	Size of effect (kHz)	
	Reference	Cs D_1
1. Optical pumping and radiation pressure	10	10
2. Stray magnetic fields	10	9
3. Laser lock to peak center	7	7
4. Collisional shifts	10	10
5. Differential phase shift at mirrors	–	15
6. Misalignment into cavity (higher-order modes)	5	5

known precisely (with few kHz accuracy). To the extent that different hyperfine peaks have different degrees of systematic error (e.g. due to optical pumping, lineshape distortion, stray magnetic fields, lock-point definition, etc.), the variation in the measured frequencies will reflect the total systematic error in the reference laser. In addition, changing the lock point of the reference laser changes the cavity mode number and the measured AOM offset. This checks for geometric alignment errors since the direction of the beam entering the cavity varies slightly with the frequency. The total error in the data also reflects the statistical error in the unknown and reference lasers. However, any systematic error in the unknown laser does not show up in the data because we are measuring the same transition and looking only at the variation around the mean.

In earlier work [16], we have shown that the total uncertainty in such a set of measurements is less than 30 kHz. Therefore, our estimate of 20 kHz for the total systematic error in the reference laser (adding the errors in Tab. 1 in quadrature) is quite reasonable. In reference [15], where the absolute frequency of the Rb reference transition was measured, the laser was similarly locked using saturated-absorption spectroscopy in a room-temperature vapor cell. The intensities in the pump and probe beams were similar to our values. Under these conditions, they found that the laser could be locked to line center with an uncertainty <3 kHz. Therefore, our total uncertainty of 20 kHz again appears reasonable.

For the Cs laser, we can similarly check our estimate of systematic errors by measuring different hyperfine transitions. Again, to the extent that different transitions have different systematic errors, the variation in the data will reflect the total error in the measurement. This analysis is presented in the next section where we discuss our results.

4 Results and discussion

The measured frequencies of various hyperfine transitions in the D_1 line are listed in Table 2. To check for any long term drifts, the measurements were repeated over a period of two months. In addition, the measurements were done with different lock-points of the reference laser. The final values listed each have a statistical error of less than 5 kHz. The total systematic error from Table 1 is 31 kHz. All the frequencies (which are 114 nm away from the reference wavelength) have been measured at two cavity lengths: $L_1 = 226$ mm and $L_2 = 178$ mm. Within the accuracy of the measurements, there is no significant difference between the two sets of values, hence we do not need to correct for dispersion effects at the cavity mirrors using equation (2).

Table 2. Measured frequencies of various hyperfine transitions in the D_1 line. The first set of values is for a cavity length of $L_1 = 226$ mm, while the second set is for a cavity length of $L_2 = 178$ mm. The statistical error is less than 5 kHz.

D_1 Transition	Measured frequency (MHz)	
	L_1	L_2
$F = 4 \rightarrow F' = 4$	335 112 537.916	335 112 537.892
$F = 4 \rightarrow F' = 3$	335 111 370.236	335 111 370.225
$F = 3 \rightarrow F' = 4$	335 121 730.539	335 121 730.504
$F = 3 \rightarrow F' = 3$	335 120 562.862	335 120 562.842

Table 3. Consistency check 1. The frequency difference between transitions from the two ground levels ($F = 3$ and 4) to the same upper level (F') should match the ground-hyperfine interval listed on line 1.

	Hyperfine interval (MHz)
Definition of second	9 192.632
$F' = 3$, at L_1	9 192.626
$F' = 4$, at L_1	9 192.623
$F' = 3$, at L_2	9 192.617
$F' = 4$, at L_2	9 192.612

4.1 Consistency checks

There are two kinds of internal consistency checks that we do on the data, as illustrated below.

(i) The frequency of transitions to the same excited state from different ground states should differ by the ground hyperfine interval. In the case of Cs, the ground hyperfine interval is used in the definition of the second, and is *specified* to be 9192.63177 MHz. The measured intervals from 4 transitions are listed in Table 3. All of them lie within 20 kHz of the correct value. Note that this is a powerful check on systematic errors because in most other atoms also the ground state hyperfine intervals are known with sub-kHz precision [24].

(ii) The second check on the data, as mentioned in the previous section, is that the different hyperfine transitions should yield the same value (within the total error) for the hyperfine-free frequency of the line center. For the $6P_{1/2}$ state, the hyperfine constant A is not known previously [2,28] with sufficient precision to allow an independent check. Rather, our measurements improve the knowledge of A, as discussed in the next section. However, we can check for internal consistency among the eight measurements since

Table 4. Consistency check 2. The different transitions measured should yield the same value for the hyperfine-free frequency of the line center. The average value is 335 116 048.817 MHz.

Transition	Hyperfine-free frequency (MHz)	
	L_1	L_2
$F = 4 \rightarrow F' = 4$	335 116 048.835	335 116 048.811
$F = 4 \rightarrow F' = 3$	335 116 048.828	335 116 048.817
$F = 3 \rightarrow F' = 4$	335 116 048.827	335 116 048.792
$F = 3 \rightarrow F' = 3$	335 116 048.823	335 116 048.803

there is only one hyperfine interval. The hyperfine-free frequencies obtained from each transition (using our value of A) are listed in Table 4, and are quite consistent with the average value. Again, it is important to note that in many other atoms the hyperfine constants in the excited states are already known with high precision, and this can be another powerful check on the measurements.

4.2 Hyperfine structure

As mentioned above, we can use our data to obtain the hyperfine interval in the excited state. The interval is measured with an accuracy of 30 kHz. Note that many sources of systematic error cancel in measuring this difference frequency. For example, any systematic shift of the reference laser will affect all the measured frequencies equally. Similarly, collisional shifts will be the same for all hyperfine components and will cancel in the difference.

Our result is compared to earlier results from references [2,28] in Figure 6. Our value is consistent but has better accuracy. The measured interval can be expressed as $4A$, where A is the magnetic-dipole coupling constant in the $6P_{1/2}$ state. The value of the hyperfine constant is therefore:

$$A = 291.918(8) \text{ MHz}.$$

4.3 Center frequency

Using the data in Table 4, we can obtain the hyperfine-free frequency of the D_1 line. The average value from the 8 measurements is:

$$6P_{1/2}{-}6S_{1/2}\text{: } 335\ 116\ 048.817(31) \text{ MHz}.$$

The final error of 31 kHz is the total systematic error for each value from Table 1, including the error in the reference laser. The standard deviation for the 8 values is 14 kHz. As mentioned in the section on error analysis, to the extent that different hyperfine transitions have different degrees of systematic error, the standard deviation in the data should reflect the total error. This shows that our estimate of 31 kHz is reasonable. Note also that the Zeeman shift is in opposite directions for the $F = 3 \rightarrow F' = 4$ transition and the $F = 4 \rightarrow F' = 3$ transition, and should cancel to some extent in the average. The above value is also consistent with the value of 335 116 048.807(41) MHz measured using the frequency-comb technique [2].

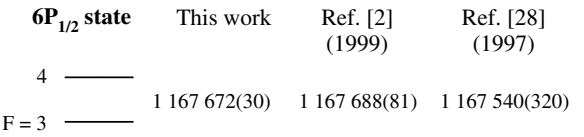

Fig. 6. Hyperfine interval in the $6P_{1/2}$ state of ^{133}Cs. The measured interval (in kHz) in the current work is compared to earlier work.

5 Conclusion

In conclusion, we have described in detail a technique for measuring the absolute frequencies of optical transitions. The frequency is compared against a reference transition in Rb using a ring-cavity resonator. The primary advantage of the technique is that the reference frequency can be varied over a range of several GHz to check for certain kinds of systematic errors. Potential systematic errors due to dispersion effects are eliminated by evacuating the cavity and repeating the measurement at different cavity lengths. We have considered several other sources of systematic errors, and shown that they are all under control.

We have applied the technique to frequency measurements on the D_1 line of Cs. We demonstrate a precision of 31 kHz for the center-of-gravity of the line, which is similar to the precision obtained for the same line using the frequency-comb technique. This measurement is important for a new sub-ppb determination of the fine-structure constant. We have recently also completed similar measurements on the Cs D_2 line. The measurement on the D_2 line is complicated because the lineshape in saturated-absorption spectroscopy is much more susceptible to distortion due to the effects of stray magnetic fields and pump power, as shown in reference [29]. These effects have limited our accuracy in determining the center-of-gravity to 55 kHz, even though we can measure (and average over) 10 independent hyperfine components. The final value of 351 725 718.509(55) MHz is consistent with the value of 351 725 718.500(110) MHz measured using the frequency-comb technique in reference [6]. A more recent measurement with the frequency comb in reference [7] has a much higher accuracy of 5 kHz, obtaining a value of 351 725 718.4744(51) MHz.

While we have achieved the above precision for the Cs lines whose natural linewidth is 5 MHz, it should be possible to achieve better accuracy for narrower lines. One fundamental limit to our technique is clearly the precision of 6 kHz with which the reference transition is known. However, it is possible to improve this quite easily by using the nearby two-photon transition in Rb ($5S_{1/2} \rightarrow 5D_{5/2}$ transition at 778 nm) as the reference. This transition has a natural linewidth of only 600 kHz and its absolute frequency has been measured with 2 kHz accuracy [30].

This work was supported by the Department of Science and Technology, Government of India. Two of us (D.D. and S.B.) acknowledge financial support from the Council of Scientific and Industrial Research, India.

References

1. A good review of laser cooling and trapping experiments is contained in the Nobel Prize lectures: S. Chu, Rev. Mod. Phys. **70**, 685 (1998); C.N. Cohen-Tannoudji, Rev. Mod. Phys. **70**, 707 (1998); W.D. Phillips, Rev. Mod. Phys. **70**, 721 (1998)
2. T. Udem, J. Reichert, R. Holzwarth, T.W. Hänsch, Phys. Rev. Lett. **82**, 3568 (1999)
3. A. Banerjee, D. Das, V. Natarajan, Europhys. Lett. **65**, 172 (2004)
4. D.S. Weiss, B.C. Young, S. Chu, Phys. Rev. Lett. **70**, 2706 (1993)
5. M.P. Bradley, J.V. Porto, S. Rainville, J.K. Thompson, D.E. Pritchard, Phys. Rev. Lett. **83**, 4510 (1999)
6. T. Udem, J. Reichert, T.W. Hänsch, M. Kourogi, Phys. Rev. A **62**, 031801R (2000)
7. V. Gerginov, C.E. Tanner, S. Diddams, A. Bartels, L. Hollberg, Phys. Rev. A **70**, 042505 (2004)
8. A. Peters, K.Y. Chung, S. Chu, Nature **400**, 849 (1988)
9. C.S. Wood, S.C. Bennett, D. Cho, B.P. Masterson, J.L. Roberts, C.E. Tanner, C.E. Wieman, Science **275**, 1759 (1997)
10. C. Chin, V. Leiber, V. Vuletić, A.J. Kerman, S. Chu, Phys. Rev. A **63**, 033401 (2001)
11. G.P. Barwood, P. Gill, W.R.C. Rowley, Appl. Phys. B **53**, 142 (1991)
12. J. Walls, R. Ashby, J.J. Clarke, B. Lu, W.A. van Wijngaarden, Eur. Phys. J. D **22**, 159 (2003)
13. H. Liening, Z. Phys. A **320**, 363 (1985)
14. T. Loftus, J.R. Bochinski, T.W. Mossberg, Phys. Rev. A **63**, 023402 (2001)
15. J. Ye, S. Swartz, P. Jungner, J.L. Hall, Opt. Lett. **21**, 1280 (1996)
16. A. Banerjee, D. Das, V. Natarajan, Opt. Lett. **28**, 1579 (2003)
17. A. Banerjee, Ph.D. thesis, Indian Institute of Science, Bangalore, unpublished (2004)
18. A. Banerjee, U.D. Rapol, D. Das, A. Krishna, V. Natarajan, Europhys. Lett. **63**, 340 (2003)
19. D. Das, S. Barthwal, A. Banerjee, V. Natarajan, Phys. Rev. A **72**, 032506 (2005)
20. A. Banerjee, U.D. Rapol, A. Wasan, V. Natarajan, Appl. Phys. Lett. **79**, 2139 (2001)
21. A.J. Wallard, J. Phys. E **5**, 926 (1972)
22. H. Kogelnik, T. Li, Appl. Opt. **5**, 1550 (1966)
23. A. Banerjee, D. Das, U.D. Rapol, V. Natarajan, Appl. Opt. **43**, 2528 (2004)
24. E. Arimondo, M. Inguscio, P. Violino, Rev. Mod. Phys. **49**, 31 (1977)
25. R. Grimm, J. Mlynek, Appl. Phys. B **49**, 179 (1989)
26. Conetic AA Alloy, Magnetic Shield Division, Perfection Mica Co., USA
27. A.E. Siegman, *Lasers* (Oxford University Press, Oxford, 1986)
28. R.J. Rafac, C.E. Tanner, Phys. Rev. A **56**, 1027 (1997)
29. O. Schmidt, K.M. Knaak, R. Wynands, D. Meschede, Appl. Phys. B **59**, 167 (1994)
30. D. Touahri, O. Acef, A. Clairon, J.J. Zondy, R. Felder, L. Hilico, B. de Beauvoir, F. Biraben, F. Nez, Opt. Commun. **133**, 471 (1997)